DOI: 10.4408/IJEGE.2013-06.B-58

EXPLORATION OF THE KINEMATICS OF THE 1963 VAJONT SLIDE, ITALY, USING A NUMERICAL MODELLING TOOLBOX

Andrea WOLTER(*) , Mohsen HAVAEJ(*), Luca ZORZI(**), Doug STEAD(*), John J. CLAGUE(*), Monica GHIROTTI(***)& Rinaldo GENEVOIS(****)

(*)Simon Fraser University - Burnaby, British Columbia, Canada
(**)Golder Associates- Burnaby, British Columbia, Canada
(***)Alma Mater Universitá di Bologna - Bologna, Italy
(****)Universitá degli Studi di Padova - Padova, Italy

ABSTRACT

The Vajont Slide has been studied for half a century, yet questions about its kinematics and dynamics still remain. Application of state-of-the-art numerical techniques aids in understanding the slide's mechanical behaviour. In the current paper, we use four two- and three-dimensional finite element, distinct element, and lattice-spring modelling codes in a toolbox approach to conduct a forensic, exploratory investigation of the kinematics of the slide. We examined the influence of rock mass properties and friction along the failure surface using the 2D finite element code. Preliminary results indicate that weaker units within the sliding mass deformed more than stronger units, and that a Prandtl wedge zone of transition developed between the active upper and passive lower blocks of the slide mass in the west. The difference between the biplanar western sliding surface and the more circular eastern surface proves to be significant in terms of stability. Models suggest a critical friction angle of approximately 18°, above which the slope is stable. The 2D distinct element modelling results indicate that both failure surface morphology and block size are important. Planar and arc-shaped failure surfaces are most unstable, whereas rough undulating surfaces are stable. As block size increases, overall slope stability increases and a lower friction angle along the failure surface is required to initiate sliding. Block kinematics were further investigated using a 3D distinct element code. This numerical code illustrated the controls of bounding structural features such as the Col Tramontin Fault and Erto Syncline, as well as block size, on the failure. Finally, preliminary simulations in a new 3D lattice-spring code show that crack clusters developed, and became concentrated in the transition zone between the back and seat of the chair-shaped failure surface.

Key words *Vajont Slide; kinematics; numerical modelling; toolbox approach; finite element; distinct element; lattice-spring*

INTRODUCTION

The 1963 Vajont Slide, Italy is one of the most devastating and significant landslides in history. Although extensively researched over the past 50 years, certain aspects of this catastrophic failure remain unknown. In particular, numerical modeling methods have been under-utilised in better understanding the kinematics and dynamics of the failure. Most analyses of the slide have employed a limit equilibrium approach and have only considered two dimensions. The first model of Vajont was a 1:200 scale physical model constructed in 1961 to investigate the effects of a potentially catastrophic failure and resulting displacement wave on the area (Semenza, 2010). Since then, few scientists have researched the displacement wave; for example, Bosa & Petti (2011), Ward & Day (2011) and Vacondio *et alii* (in this volume) show numerical simulations of the wave. In one of the seminal works on Vajont, Hendron & Patton (1985) conducted the first three-dimensional stability analysis of the Vajont Slide. Ghi-

 © 2013 Sapienza Università Editrice

ROTTI (1992; 1994) and SITAR & MACLAUGHLIN (1997) completed the first two-dimensional numerical models of the slide, but little further modeling work has been conducted until recently. In connection with the 50th anniversary conference, several researchers, including CASTELLANZA *et alii* (in this volume) and HUNGR (in this volume) have contributed two- and three-dimensional numerical models.

Although most of the modelling published has been conducted in two dimensions, the Vajont Slide is without doubt a three-dimensional problem. Two-dimensional cross-sections neglect the structural and morphological differences across the failure surface, such as the bowl-shaped failure surface, upstream plunge of one of the synclines defining the sliding surface, and the change in its geometry from a chair shape in the west to a circular surface in the east. Most modelling results have also been interpreted as rigorous indicators of mobilised shear strength and slide displacement, rather than as aids in understanding the kinematics of slide behaviour and an exploration of different mechanisms and hypotheses.

Sophisticated analyses of the Vajont Slide demand a relatively large data set. Despite the many studies and publications on Vajont, relatively few researchers discuss or attempt to quantify sliding surface and rock mass properties, and those that do commonly cite different values. This issue becomes apparent when attempting to input parameters into modeling software. GHIROTTI (1992) bases input parameters on seismic velocities of the failed rock mass as estimated by MARTINIS (1978), and on published parameter values for limestone (BANDIS *et alii*, 1983). She is one of the few workers to consider the effects of water directly within numerical models, but does not explicitly consider the clays along the shear surface. SITAR & MACLAUGHLIN (1997) base their 2D Discontinuous Deformation Analyses (DDA) of block size effects on elastic modulus and Poisson's ratio, but do not provide the numerical values they used or the source of the values. Only SUPERCHI (2012) provides field estimates and laboratory test results of rock mass and intact rock strengths.

If the hypothesis that the landslide mass behaved as several large intact blocks is accepted, the slope rock mass properties may be less relevant than those of the failure zone in understanding the failure. In this context, the properties of the clay layers and previously failed material, such as the cataclasite mentioned by HENDRON & PATTON (1985), may be important. Numerous studies discuss the clay properties, but only HENDRON & PATTON (1985), TIKA & HUTCHINSON (1999), and FERRI *et alii* (2011) have published laboratory results of geomechanical properties. Several of the original reports, such as MÜLLER (1968) neglected the clays, as they were thought to be insignificant.

At present, a still debated characteristic of the Vajont Slide is the thickness of the shear zone. The generally accepted model is that hypothesised by Rossi and Semenza (in HENDRON & PATTON 1985) based on cross-sections which show a discrete primary failure surface and several secondary shear surfaces. Recently, PARONUZZI & BOLLA (2012) proposed that the shear zone could have been over 100 m thick.

In this paper, we provide the preliminary results of four, two- and three-dimensional numerical codes used in a forensic analysis of the kinematics of the Vajont Slide. None of the models should be interpreted as an accurate representation of actual conditions, but rather as an aid in examining the effects of different material properties, discontinuity networks, and slope geometries on failure. Although groundwater, a critical aspect of the Vajont Slide, is not explicitly considered in these preliminary simulations, we approximate its effects by using low friction properties along the failure surface and discontinuities. We take a toolbox approach and highlight the challenges and uncertainties associated with modelling a failure with such complex geometry, mechanisms, and behaviour.

BACKGROUND

The Vajont River has eroded a carbonate-dominated sequence of limestones interbedded with marl, clay, and clastic rocks. The Vajont Slide involved Jurassic-Cretaceous units within the Fonzaso Formation and Calcare di Soccher, which overlie the Calcare del Vajont. The Calcare di Soccher is further divided into six units – A to F – that include fossiliferous limestone, biomicrite, marl, and conglomerate. In terms of geotechnical properties, the Fonzaso Formation and unit A of the Calcare di Soccher can be considered one material and units C to F of the Calcare di Soccher another. The conglomerate (unit B) is distinguished from the other Soccher units (Rossi and Semenza maps in HENDRON & PATTON, 1985). The deposit material in the east is more disturbed and weaker than that in the west (Fig. 1a and b), and is densely vegetated, with a fine matrix sepa-

rating clasts of a variety of sizes. The material in the west remained more competent as it failed and generally has a higher strength; it remained relatively intact and preserved stratigraphy. This difference may be due to the influence of the Col Tramontin Fault on rocks in the east.

The Vajont Slide is bounded and kinematically controlled by several discontinuities and sets of folds (Fig. 1). Two faults delimit the eastern lateral scarp and the western headscarp – respectively, the Col Tramontin Fault and Col delle Erghene Fault. An analysis of long-range terrestrial digital photogrammetric models (Wolter *et alii*, submitted) indicates that the orientations of these two structures are 59°/283° (dip/dip direction) and 55°/010°, in agreement with results of other studies (Superchi, 2012; Massironi *et alii*, in this volume). The discontinuities define an asymmetrical sliding mass with a characteristic M-shape.

The north slope of Monte Toc, which defines the south-west wall of the Vajont Valley, has been deformed by the Massalezza and Erto synclines and associated parasitic folding related, respectively, to the Dinaric and Neo-Alpine tectonic events. The Massalezza Syncline is a recently discovered feature that contributes to the bowl shape of the failure surface (Massironi *et alii*, in this volume; Wolter *et alii*, sub-

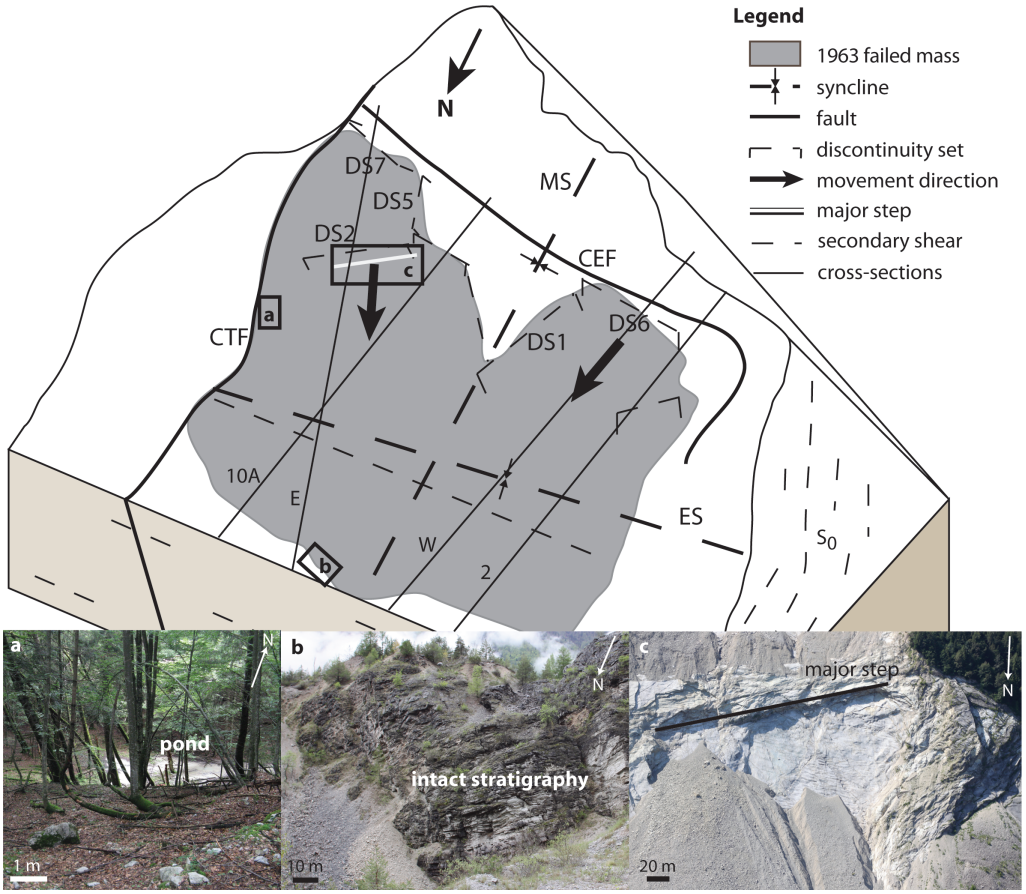

Fig. 1 - Block model illustrating the structures that define the Vajont Slide. DS=discontinuity set, CTF=Col Tramontin Fault, CEF=Col delle Erghene Fault, ES=Erto Syncline, and MS=Massalezza Syncline. Cross-sections 2 and 10A are from Hendron & Patton (1985) and cross-sections W and E from are Bistacchi et alii (in this volume). Note that the E and W sections roughly parallel the directions of movement. Insets a) and b) show the difference in character between the deposits of the east block (densely vegetated, with ponding, clasts of a range of sizes, and a fine matrix) and the west block (relatively intact rock with stratigraphy preserved). Inset c) illustrates the major step in the east-central area of the failure scar, which we used as a boundary between the east and west blocks (see text)

 © 2013 Sapienza Università Editrice

mitted). Its axis plunges to the north. The Erto Syncline, the southern limb of which forms the characteristic chair-shaped profile of the failure surface, plunges approximately 20° east and defines the axis of the Vajont Valley. Both fold systems interact with each other to produce complex dome-and-basin to crescent-and-mushroom interference patterns (Massironi *et alii*, in this volume). These interference patterns are apparent over most of the present-day failure scar, and may have played an important role in the failure.

The failure scar geometry is further complicated by step-paths associated with folding-related discontinuities that are separated by areas of intact rock. Steps in the failure scar are oblique to the sliding direction and could act as release surfaces for smaller rock masses. The step in the east-central area is an example (Fig. 1c). Hendron & Patton (1985) hypothesised that, although the failure surface predominantly follows bedding in the west, with minor steps between beds, it steps up to ground level in the east.

Superchi (2012) and Bistacchi *et alii* (in this volume) propose that the Vajont Slide moved as two main blocks, an east and a west block. An approximate reconstruction of the failure deposit shows that the location of the boundary between these blocks is a parasitic fold complex and a large step located in the east-central area of the failure scar (Fig. 1c). Although the step is not apparent on pre-failure aerial photographs or on photographs taken immediately after the 1963 slide, we tentatively identify it as the approximate boundary between the east and west blocks.

Other block boundaries may have been discontinuity sets, the Massalezza Gully, and secondary shear surfaces, as seen on Rossi and Semenza's cross-sections (in Hendron & Patton, 1985). Although the Massalezza Gully remained intact during sliding, we used it as a boundary to observe how it may have affected initial pre-failure block kinematics if it were a release surface.

EFFECT OF MATERIALS AND STRENGTH ON FAILURE IN 2D FINITE ELEMENT ANALYSES

METHODOLOGY AND MODEL PROPERTIES

We conducted initial investigations of failure behaviour and rock mass parameters using Phase2 (Rocscience, 2012), a 2D finite element code that uses the Shear Strength Reduction (SSR) technique to model the degradation of rock and soil materials as well as discontinuity properties. This technique reduces the strength parameters of a slope by a Strength Reduction Factor (SRF) until it fails and determines the critical SRF, equivalent to the factor of safety, at failure. We first ran models with different materials using Rossi and Semenza's Section 2 (Hendron & Patton, 1985). The purpose was to observe the effects of changes in material properties on internal deformation of the sliding mass. Second, we varied the friction angle along the Section 2 failure surface from 38° to 5° to investigate the stability of the sliding mass along a discrete surface. Finally, we used four cross-sections to investigate the effects of slope and failure surface geometry on model stability in Phase2: Rossi and Semenza's Sections 2 and 10A (Hendron & Patton, 1985) and Bistacchi *et alii* (in this volume) updated east and west sections (see Fig. 1 for section locations).

Table 1 lists the rock mass and discontinuity properties used in all codes, based primarily on Ghirotti (1992). All models include the specified failure surface, because the purpose of the modelling was to back-analyse the existing Vajont Slide. One joint material (jmat 1) was applied to all discontinuities in most models. A second set of joint properties (jmat 2) was applied to sub-vertical discontinuities in some models (faults, discontinuity sets, etc., as seen below) to determine their effect on stability.

PRELIMINARY RESULTS

Internal deformation of the sliding mass in the Phase2 models was concentrated within the zone of transition between the active back and passive seat of the chair-shaped failure surface, supporting Mencl's (1966) Prandtl wedge hypothesis. Three zones of high-

Parameter	Vajont	Fonzaso, A	Unit B	Units C-
Density (kg/m^3)	2690	2700	2700	2610
Rock mass modulus (GPa)	9.0 - 40.0	3.9	8.4	6.1
Tensile strength (MPa)	3-5	n/a	n/a	2.5
Poisson's ratio	0.25	0.25	0.25	0.25
Bulk modulus (GPa)	6.14	2.66	5.68	4.15
Shear modulus (GPa)	3.68	1.6	3.41	2.49
Friction angle (°)	45	40	45	40
Cohesion (MPa)	n/a	0.1	n/a	0.1

Parameter	Jmat 1	Jmat 2
Friction angle (°)	0 - 40	30
Cohesion (MPa)	0 - 0.05	0.01
Joint normal stiffness (GPa/m)	5	5
Joint shear stiffness (GPa/m)	0.6	0.6

Tab. 1 - Properties used for the two- and three-dimensional models, based on Ghirotti (1992). The Vajont limestone was used in all one-material models, unless otherwise noted

er shear strain occur at breaks in slope of the failure surface in all models (Fig. 2). The angles, measured from horizontal, of each potential shear range from 45° to 90°. The thickest shear zone in each model, approximately 80 m wide, is inclined about 70°, and is located in the Prandtl wedge zone. Models with weaker materials show an additional semicircular incipient shear zone inclined about 45° at the front of the unstable mass (indicated by a black box in Fig. 2b). This result may indicate a secondary failure, similar to the November 1960 failure. Thus, the weaker material models show more internal deformation in the rock mass than the stronger material models, as might be expected. Assuming that the failure surface has a friction angle of 12°, the anticipated shear surface angles within the rock mass are between 39° and 51°, given the equation $\theta = 45° \pm \varphi/2$, where θ is the expected angle of the failure surface and φ is the friction angle along that plane. The secondary semicircular shear zones in the weaker material models fall within this range. Higher angles of potential shear zones require friction angles of at least 77°. If the inclination of the failure surface in the upper part of the slope, at 20° to 40°, is taken into account, the other shear zones also fall within the given range for $\varphi = 12°$.

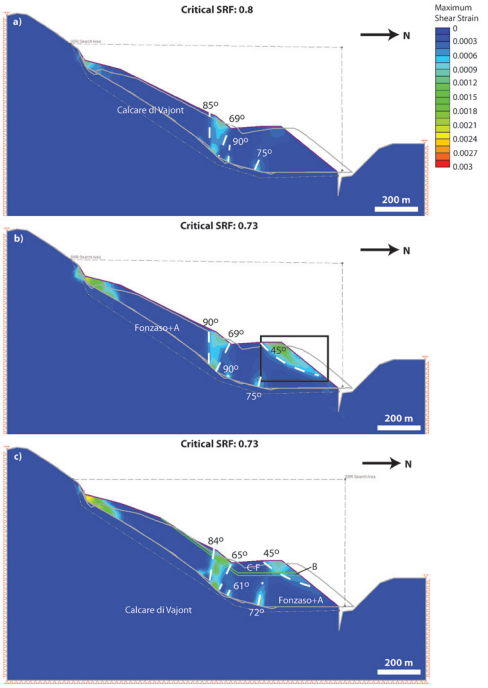

Fig. 2 - Preliminary results based on Phase2 models. Maximum shear strain plots of a) one-material model based on the Calcare di Vajont, b) one-material model based on the Fonzaso Formation and Unit A material, and c) four-material model including the Calcare di Vajont, the Fonzaso Formation, and Units A, B, and C-F of the Soccher Formation. Dashed white lines and angles (from horizontal) indicate potential shear zone characteristics. The dashed grey box outlines the search area used for the SSR analyses. The significance of the black box in b) is discussed in the text

The four-material models further illustrate the effect of material properties. Ghirotti (1992; 1994) illustrated the importance of the stronger, more brittle conglomerate layer (Unit B of the Soccher Formation) in keeping the rock mass relatively intact. Although no such conclusions can be drawn from the preliminary Phase2 results, there is less shear strain concentrated within this thin layer than in the weaker materials surrounding it, supporting Ghirotti's (1992; 1994) conclusion (Fig. 2c).

As we reduced the friction angle along the failure surface, the critical Strength Reduction Factor (SRF), and thus stability, decreased. The correlation between friction angle and SRF appears to be linear (Fig. 3). The critical friction angle was determined to be 18°, above which the slope was stable.

The different results derived from the east and west cross-sections indicate the complex nature of the Vajont failure. Rossi and Semenza's Section 2 and the west section of Bistacchi *et alii* (in this volume) show a biplanar failure with the Prandtl wedge zone separating the active back block and passive front block of the sliding mass (Fig. 2). In contrast, the east sections only show shear strain concentrations at the toe of the unstable mass. Rossi and Semenza's Section 10A has a slightly higher

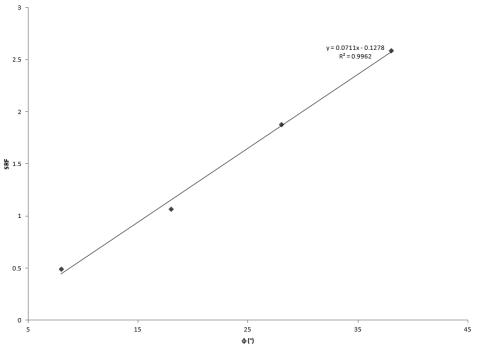

Fig. 3 - Linear relationship between the friction angle (φ) along the failure surface and Strength Reduction Factor (SRF) in Phase2 as the friction angle is increased over the failure surface

 © 2013 Sapienza Università Editrice

critical SRF than Section 2 (SRF=0.75 versus 0.73). The failure surface in the east section of BISTACCHI *et alii* (in this volume) dips more steeply than that of the west section and is thus less stable; it approximates a linear or curved surface rather than a chair-shaped surface. If only this section were analysed, the stability of the slope would be significantly underestimated. The east block failed last, hence it would give a false impression of failure if analysed alone. A 2D section cannot simulate the interactions between the east and west blocks as it neglects variations in kinematic freedom in the third dimension. The results may, however, indicate the different potential mechanisms of failure in the east and west, in a situation where the west block moved to provide kinematic freedom for the east block.

IMPORTANCE OF FAILURE SURFACE MORPHOLOGY AND BLOCK SIZE IN 2D DISTINCT ELEMENT MODELS

METHODOLOGY AND MODEL PROPERTIES

UDEC (Universal Distinct Element Code; ITASCA, 2012c) is a two-dimensional discontinuum code used to model a variety of rock engineering problems. We used this code to investigate the importance of failure surface morphology and failure mass block size. Using Rossi and Semenza's Section 2 and GHIROTTI'S (1992) material properties for rigid blocks comprising one and four materials (Tab. 1), we tested a variety of failure surface geometries involving planar, arc-shaped, biplanar, and undulating surfaces, as well as Rossi and Semenza's original failure surface. Undulating surfaces were used to assess the potential effect of a complex failure surface on slide kinematics due to interference between the two fold generations mentioned above. Following a methodology similar to SITAR & MACLAUGHLIN (1997),we also re-examined the significance of block size and discontinuity spacing. We input sub-vertical joints into the models, and changed their spacing from 50 m to 100, 200, and 500 m.

PRELIMINARY RESULTS

The morphology of the failure surface had a strong effect on failure mechanics. We determined the approximate value of the critical friction angle for each configuration (Tab. 2). The most unstable configurations were the linear and arc-shaped failure surfaces, whereas the most stable configuration was the roughest of the three undulating surfaces. The biplanar and Rossi and Semenza failure surfaces have a similar effect on stability - the slide mass fails only when the friction angle along the slide surfaces is reduced to 5°, assuming dry conditions.

When sub-vertical joints are introduced into the one- and four-material failure masses, the critical friction angles along the Rossi and Semenza failure surface are approximately 16° and 12°, respectively, indicating a decrease in stability compared to models without joints. We observed similar decreases in stability for all other failure surfaces, except the roughest undulating surface, which remained stable. The locations of the individual joints are the same as those used by GHIROTTI (1992; 1994).

Using the Rossi and Semenza failure surface and four materials, we found that as the spacing of the sub-vertical joints and thus block size increased, the failure mass stabilised and thus the friction angle required to induce failure decreased. These results are similar to SITAR & MACLAUGHLIN'S (1997) observations using Discontinuous Deformation Analysis (DDA). An active-passive mechanism, rather than uniform sliding, became evident when block size was increased (Fig. 4). As block size increased, the lower blocks became passive, and a more obvious Prandtl wedge developed between the active and passive blocks where shear

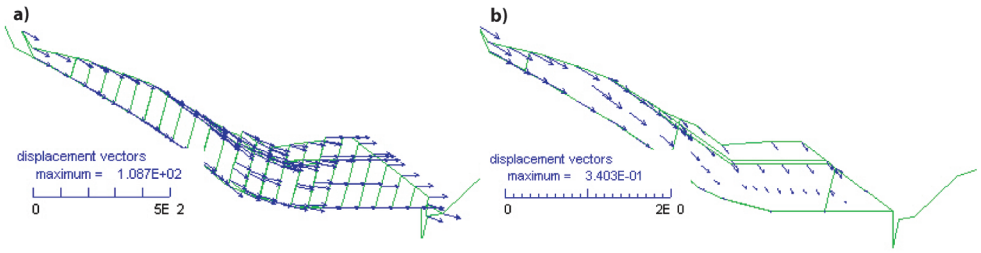

Fig. 4 - Increasing stability as block size is increased in UDEC. a) Sub-vertical joint spacing is 50 m, and b) sub-vertical joint spacing is 500 m. The failure mode changes from uniformly sliding to active-passive, accompanied by a significant decrease in displacement

stress and shear strain were localised. Block size thus has important implications for the modelling of the Vajont failure mechanism.

3D–DISTINCT ELEMENT MODEL ANALYSES TO INVESTIGATE BLOCK KINEMATICS

METHODOLOGY AND MODEL PROPERTIES

3DEC (ITASCA, 2012a), a 3-Dimensional Distinct Element code that applies an explicit solution scheme to problems in discontinuous media, was used to investigate simple block kinematics and interactions at Vajont. The geometry of the simulations is based on the GoCAD model of Bistacchi *et alii* (in this volume). The actual topography is too complex to import directly into 3DEC for the purposes of our preliminary kinematic modelling; thus we used it to simplify the topography by approximating it with intersecting planes (Fig. 5). We also started with the simplest possible model, so that an appreciation of the kinematic controls of the event could be obtained without the complication of "topographic noise" or unnecessary model complexity.

We used a variety of different 3DEC model geometries with different kinematics. Initial models were created without the Massalezza Gully catchment basin to compare with those that included it (Fig. 5). The dip of the part of the basal plane defining the seat of the chair-shaped failure surface between the Col Tramontin Fault and the east-plunging Erto Syncline was varied from 0° to 5° and 10° to the north. The dips and dip directions of the planes representing i) the Col Tramontin Fault, which forms the east lateral boundary, ii) the southern limb of the Erto Syncline, which forms part of the basal surface, and iii) the two limbs of the Massalezza Syncline, which form the rear release or back of the chair, were varied to ±20° of the values derived from photogrammetric analyses (Wolter *et alii*, submitted) in models including a basal plane dipping 5° and a discontinuity set spaced at 200 m. We also varied the number of blocks. Models first were run with the entire landslide mass forming one block. Then, discontinuities related to structural features were added to cut the landslide mass into two or more blocks. The discontinuities include a major step in the central-east area of the failure scar that is associated with folding, the Massalezza Gully, and hypothesized secondary shear surfaces. Finally, we added regularly spaced discontinuity sets to observe the effect

Model	Critical φ (°)
Linear	12
Circular	13
Biplanar	5
Undulating	stable
Rossi and Semenza	5

Tab. 2 - Critical friction angle for the different sliding surface configurations in UDEC, assuming dry conditions

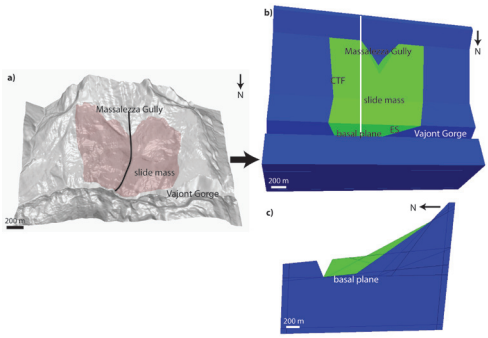

Fig. 5 - Simplification of a) the complex topography supplied by Bistacchi et alii (in this volume) for use in 3DEC. b) Plan view. c) Cross-section along the white line in b). Structural features are represented by planes. CTF=Col Tramontin Fault. ES=north limb of Erto Syncline. The basal plane connects the Col Tramontin Fault and Erto Syncline

of block size (Figs. 1 and 6). The method approximately follows that employed by Corkum & Martin (2004) in their investigation of a dam abutment rock slope near Revelstoke, BC, Canada.

We chose a rigid block model assuming that the sliding material remained intact and that discontinuity properties dominated failure. We assumed Coulomb-slip area contact constitutive behaviour for all discontinuities and performed sensitivity analyses on the friction and cohesion parameters. Two sets of joint properties, jmat 1 and jmat 2, were introduced in some models to observe the effects of discontinuity properties on stability (Tab. 1). We first assigned to all discontinuities the first set of joint properties, which were reduced in several stages, simulating strength degradation over time. In further models, we introduced the second set of joint properties to the back of the chair-shaped failure surface (i.e., the two surfaces representing the limbs of the Massalezza Syncline), and/or to secondary discontinuities such as the regularly spaced discontinuity sets and the plane representing the Massalezza Gully; jmat 2 properties were not changed within each model.

© 2013 Sapienza Università Editrice

PRELIMINARY RESULTS

Unlike the majority of the 2D model results, the initial 3DEC simulations were stable, as expected. The horizontal basal plane on the seat of the chair-shaped failure surface prevented significant movement until friction was decreased to zero, clearly an unrealistic scenario. The very low friction angle necessary for failure may indicate that: i) increased pore pressures contributed significantly to failure, effectively lowering the frictional resistance along the sliding surface; ii) the models require more kinematic freedom to fail, either through an increase in the number of blocks or through removal of material; or iii) the assumed model geometry is incorrect. Models with smaller blocks (see below) and dips of the basal failure plane of 5° and 10° produced significant displacements at friction angles of 5° and higher. These results suggest that block geometry and kinematic freedom are critical inputs, as would be expected. The role of groundwater, although not simulated in the preliminary models, is, as observed in practice, critical.

As in the case of the UDEC simulations, discontinuity spacing proved to be important. When the landslide mass was modelled as one block no significant movement occurred. This observation suggests that the sliding mass, although hypothesised to behave as a relatively intact, rigid body, clearly contained internal discontinuities that allowed several large blocks to move with respect to one another. Block theory (Goodman & Shi, 1985) also dictates that kinematic freedom should increase as block size decreases and keyblocks are removed. We therefore conducted a study of block size (Fig. 6). First, we segregated the failure mass into two blocks using a possible discontinuity related to folding in the east-central area and approximating the boundary between the east and west blocks of Superchi (2012) and Bistacchi *et alii* (in this volume). We then used the Massalezza Gully as the boundary between the two blocks. The discontinuity representing the Massalezza Gully affected the sliding mass more than the assumed discontinuity related to the east-central folding. Maximum displacement increased by more than three times for a one-joint-material model (Fig. 7), but only the west part of the slide mass moved; the east side was stable. The difference in behaviour between models incorporating the east-central folding discontinuity and those incorporating the Massalezza Gully may be due to the decrease in the size of the west block compared to the folding-related discontinuity model. Alternatively, the vertical discontinuity striking north-south and separating the east and west blocks perhaps provided better kinematic release than the discontinuity striking NE-SW. The observation that the 3DEC models show that the Massalezza Gully may

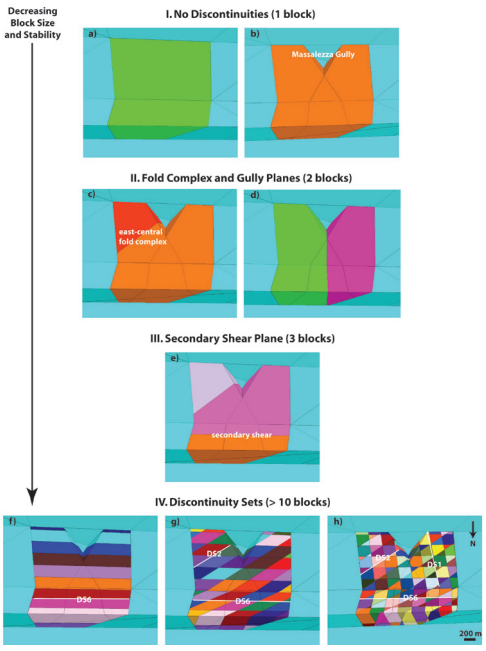

Fig. 6 - Sequence of investigation of block size and number in 3DEC. As block size decreases, stability decreases. DS=discontinuity set

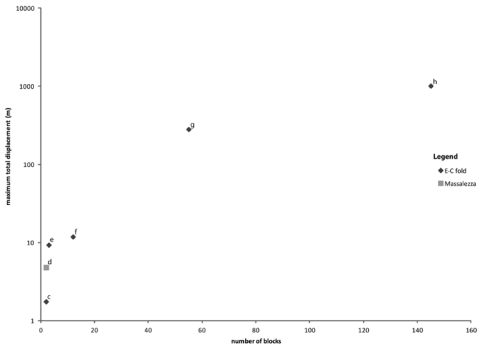

Fig. 7 - Semi-logarithmic graph of the number of blocks included in a given model versus maximum total displacement in metres. Letters correspond to those in Fig. 6. The two-block model using the Massalezza Gully (d) as a discontinuity is shown in comparison to the two-block model using the east-central fold complex (c). Note that maximum displacement is roughly three times higher in the Massalezza model. Models a and b in Fig. 6 are not plotted as they were stable

have been a more effective zone of separation for the two blocks is compelling, but contradicts post-failure observations. The sliding mass must have been competent in the Massalezza area, despite following a fold hinge. Complex fold interference patterns in that area may have also inhibited movement.

When we added a plane approximating a secondary shear surface, thus creating three blocks, the maximum displacement increased further (Fig. 7). When we added three discontinuities determined from photogrammetric analyses (Wolter *et alii*, submitted) to the model to create multiple blocks – DS1 (59°/283°, dip/dip direction), DS2 (79°/333°) and DS6 (88°/180°) – the maximum displacement increased by two to three orders of magnitudes to hundreds of metres. The simulated mechanism of movement also changed. Most two- and three-block models behaved as active-passive or uniformly sliding blocks. The blocks in the multi-block models, however, moved as separate entities with independent paths. Kinematic freedom and block size are thus important controls at Vajont, supporting the observations of Corkum & Martin (2004).

When applied to sub-vertical joints, the second set of joint properties (Tab. 1) stabilised models. The higher cohesion and friction values reduced total displacements of the slide mass by 50% to an order of magnitude. For example, in a model that included DS2 and DS6 at 200-m spacing, maximum total displacement decreased from 282 m to 127 m. These 3DEC results are preliminary and further sensitivity studies are required on stability thresholds and input parameter ranges.

The direction of displacement provides an additional indicator of model behaviour. All of the models suggest movement of the failing mass toward the NNW or NNE (Fig. 8), which is in general agreement with published vectors of movement (for example, Broili, 1967). However, some failure masses in the models initiate in the west corner, some at the west-front corner, and a few at the east corner of the headscarp, with no discernible relation to geometric trends. Maximum displacements occur most commonly in the west-front corner (Fig. 8). Thus, most models suggest failure initiation in the west, either at the deposit front (sliding) or at the headscarp (active-passive), which agrees with previous published research (Superchi, 2012; Bistacchi *et alii*, in this volume).

The number of blocks also seems to influence the displacement direction. For example, the three blocks in the model shown in Fig. 8a uniformly move to the NNE. Conversely, a multiple-block model including DS2 and DS6 (Fig. 8b) shows movement in varying directions: at the west-front corner, blocks move to the NNE; in the upper part of the west slope, they move more to the north; and in the eastern half, they move to the NNW. A simple kinematic analysis and the Hocking (1976) refinement test conducted in DIPS (Rocscience, 2012) corroborate the movement directions (Fig. 9). The east and west limbs of the Massalezza Syncline show potential for planar sliding, given a slope angle of 40° to the north and an effective friction angle of 10°. Wedge failure is possible between the east and west limbs of the Massalezza Syncline, between each limb and DS2, between each limb and the Col Tramontin Fault, and between DS2 and the Erto Syncline. Two-plane sliding could occur along the line of intersection of the two respective planes, and single-plane sliding favours one plane. Direct toppling could occur along

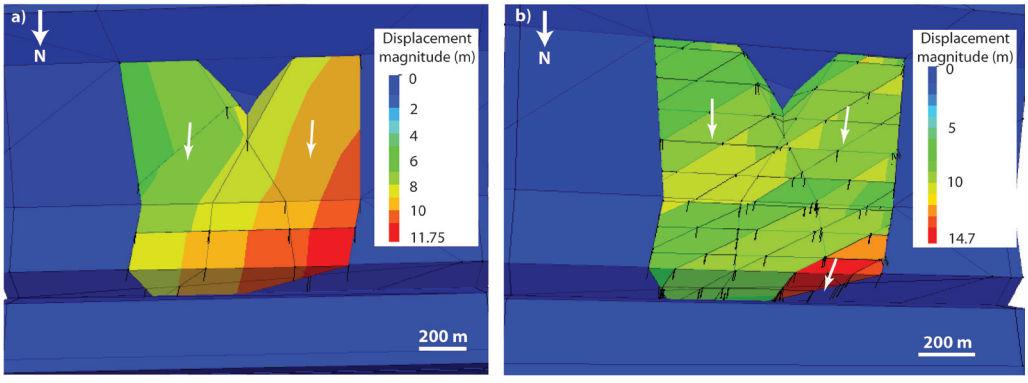

Fig. 8 - Plots of total displacement (contours) and displacement directions (black lines) for two 3DEC models. a) Three-block model including the discontinuities representing the east-central fold complex and the secondary shear plane (see Fig. 6e). b) Multi-block model including DS2 and DS6 at a spacing of 200 m (see Fig. 6g). White arrows represent general displacement directions; the arrow lengths are not to scale

© 2013 Sapienza Università Editrice

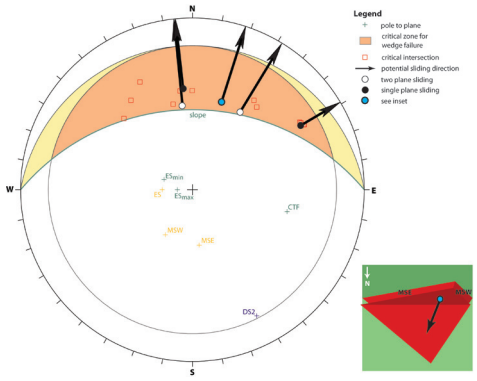

Fig. 9 - Stereonet plot showing possible wedge intersections occurring between planes included in the 3DEC models, given a slope angle of 40° to the north and an assumed low friction angle of 10°. Two- and single-plane sliding was determined using the method of Hocking (1976). Inset shows an example of a wedge between the east (MSE) and west (MSW) limbs of the Massalezza Syncline. CTF=Col Tramontin Fault, DS2=discontinuity set 2, ES=Erto Syncline, ESmin=Erto Syncline orientation yielding minimum displacement, and ESmax=Erto Syncline orientation yielding maximum displacement (see text)

planes oriented parallel to the east limb of the Massalezza Syncline. Field observations support planar and wedge failure, especially the MSE-MSW wedge seen in the inset of Fig. 9, but not toppling.

In our exploratory study of the significance of the orientations of the major planes controlling the Vajont failure, we determined that the Erto Syncline had a critical role in failure kinematics, as suggested by Hendron & Patton (1985). Varying the dip and dip direction of the plane representing the east-plunging limb of the syncline produced both the maximum and minimum total displacements in all models in our study, which included a basal plane dipping 5°, DS 6 spaced 200 m, and a friction angle of 5°. The maximum total displacement (222 m) occurred in the model with the limb of the syncline oriented at 10°/090° (dip/dip direction), and the minimum total displacement (0.28 m) occurred in the model with the syncline oriented 20°/110°. As the Erto Syncline plane is dipping into the slope in the latter case, the model is essentially stable and shows no significant movement. The former case is more difficult to interpret. In the simple kinematic analysis that we performed, assuming tetrahedral wedges, the plane is not prone to planar or wedge failure. However, it may have contributed to a complex pentahedral or hexahedral wedge or wedge-planar failure as a basal release surface, and thus would not necessarily be stable when interacting with other planes.

PRELIMINARY TENSILE FAILURE SIMULATIONS IN LATTICE-SPRING MODELS

METHODOLOGY AND MODEL PROPERTIES

Slope Model (ITASCA, 2012b) is a lattice-spring code recently developed as part of the Large Open Pit (LOP) project that simulates complex rock mass behaviour using an explicit time-stepping, discrete element approach. Slope Model incorporates the Synthetic Rock Mass (SRM) approach to simulate rock masses as a combination of intact rock and discontinuities and/or Discrete Fracture Networks (DFNs). Large-scale, important discontinuities such as faults and bedding planes should be considered separately in models. For the preliminary models in this paper, a rock mass with degraded properties was simulated with major discontinuities that intersect the sliding mass included explicitly. We used the code to investigate tensile behaviour in the Vajont failure mass, given the complex geometry of the pre- and post-failure topography (Bistacchi *et alii*, in this volume). We imposed similar block limits in these simulations as in the 3DEC models. Our models were based on one- or two-block sliding masses.

The properties used for the preliminary Slope Model simulations are listed in Table 1 and are based on accepted values for limestone, Superchi's (2012) laboratory testing, and Ghirotti's (1992) rock mass estimates. The friction angle of the discontinuities and the elastic modulus of the SRM were varied, respectively, from 10° to 45° and 9 GPa to 40 GPa. The value of 9 GPa was derived from the properties used by Ghirotti (1992; 1994). The value of 40 GPa represents a strong, granite-like rock mass, and is consistent with Superchi'S laboratory results, degraded to rock mass properties. For each model, total displacement and the number of new cracks generated were recorded to monitor failure.

PRELIMINARY RESULTS

The preliminary Slope Model simulations in which the failure mass is one continuous block and the friction angle is 13° indicate failure, unlike the one-block 3DEC simulations. When the discontinuity related to the folding in the east-central area was incorporated, displacement patterns were similar to the one-block

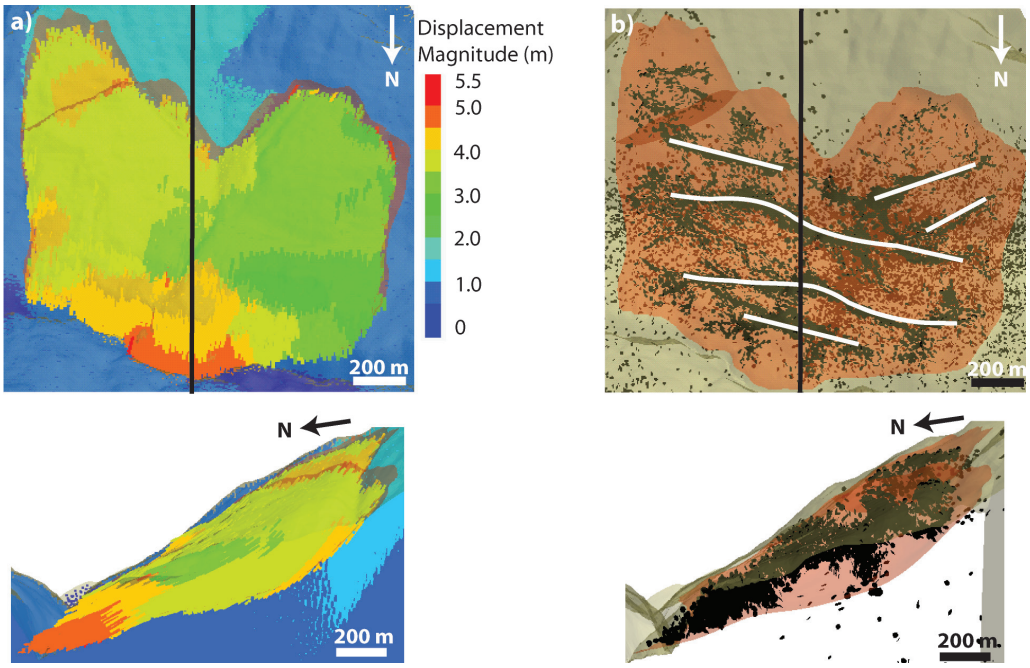

Fig. 10 - Preliminary results of a Slope Model simulation. a) Displacements in different parts of the sliding mass when separated by an assumed discontinuity related to folding in the east-central area. Black line shows location of cross-section below. b) Clusters of newly created cracks (black disks) with trends similar to those observed in the field and determined by Rossi and Semenza (in Hendron & Patton, 1985). Black line shows location of cross-section below, and white curves indicate general trends in microcrack clusters

models but tensile cracks developed in clusters trending roughly E-W (Fig. 10). These clusters are approximately parallel to the secondary shear surfaces proposed by Rossi and Semenza (Hendron & Patton, 1985) and to the compressional ridges and extensional depressions in the debris (Wolter *et alii*, in this volume). The highest concentration of newly created fractures is in the area of highest curvature between the back and seat of the chair-shaped failure surface. This result supports the Phase2 and UDEC modelling, as well as Mencl (1966), and may indicate the onset of deformation, fracturing, and disintegration of the failure mass in the Prandtl wedge zone where stress concentrations and thus deformations are expected to be highest. It may also explain why the Slope Model simulations failed, whereas the rigid 3DEC ones remained stable: the former allow internal deformation of the sliding mass and thus progressive weakening of the material.

Havaej *et alii* (2012) used the number of new cracks as an indicator of failure in their Slope Model simulation of a conceptual non-daylighting wedge failure. As the models approached equilibrium, the rate of crack formation decreased and the number of new cracks became constant (Lorig *et alii*, 2010; Havaej *et alii*, 2012). Using this cracking criterion, the critical friction angle of the Vajont slide mass is approximately 14°. With a friction angle of 15°, the slope is stable. If the friction angle of the material is reduced to 13°, displacement increases exponentially, demonstrating continued failure, and cracks continue to generate at a constant rate. The Slope Model critical friction angle is between those generated by the UDEC and 3DEC models and those of the Phase2 models. Thus, the preliminary Slope Model simulations appear slightly less stable than the UDEC and 3DEC models, but more stable than the 2D finite element models. Further work is ongoing to include DFNs in the lattice scheme in order to obtain a more realistic representation of the rock mass.

The elastic modulus value assigned to model materials affects the behaviour of those materials. A lower value represents a more ductile material and a higher modulus represents a more brittle material. The Slope Model simulations on the Vajont rock mass show this effect. Although the locations of new cracks

© 2013 Sapienza Università Editrice

changed little as the modulus of the rock mass (E_{rm}) was reduced, indicating similar stress distributions, the number of cracks decreased for a constant model run time (15 s). The material was allowed to deform more ductiley and thus there was less brittle deformation, or fracturing. The lowest E_{rm} material contained the lowest number of new cracks, and the highest E_{rm} material the highest number of new cracks. Trends in crack propagation are nonetheless similar, indicating that all models are unstable. Overall, the assumed elastic modulus, although affecting results, was not dominant. The tensile strength of the modelled rock mass was much more important to stability.

DISCUSSION AND CONCLUSIONS

All of the exploratory models presented in this paper, whether two- or three-dimensional, continuum or discontinuum, illustrate the significance of discontinuities or zones of weakness on failure. The friction angles required to produce significant movement in all models are less than or equal to 18°, indicating that the failure was controlled predominantly by weak surfaces. In all cases, significant movement required secondary shear surfaces that separated the sliding mass into multiple blocks, as suggested by Martin & Kaiser (1984). The critical friction angles obtained using Phase2 were roughly equivalent to previous values of approximately 20° (Hendron & Patton, 1985). The UDEC models suggested critical friction angles of between 12° and 16°. 3DEC critical friction angles were less than 15°, depending on block size and shape, whereas Slope Model sensitivity analyses implied a critical angle of 14°. The 3D codes generally required lower friction angles, as they considered the effects of lateral and rear release surfaces. That is, 3D models were inherently more stable than 2D simulations, and thus required lower friction angles along the sliding surface to fail. Assumptions in the preliminary models aid in explaining low friction angles. First, the simulations that treated the failed mass as one block were predominantly stable at friction angles above 5°. Second, the clays and other weak material were not explicitly included in the models; rather, they were approximated by the discontinuity properties along the failure surface. Third, as the focus for the current paper is geometry and discontinuity properties, groundwater was not explicitly considered. As many researchers have demonstrated, pore pressures within the unstable mass were clearly important. Groundwater would have reduced friction, and thus was approximated by incorporating low friction values. However, this approach does not account for important seepage forces that will be incorporated in future models. Finally, most of the models highlighted in this paper used rigid blocks. Preliminary deformable models indicate that stability decreases slightly when more complex constitutive behaviour is included.

The kinematics of the Vajont Slide are critical to realistic modelling of its behaviour. The difference between the east and west blocks highlights the three-dimensional nature of the failure. The east block appears to have failed along a circular surface and is thus less kinematically controlled than the west block. The major release plane in the east is the Col Tramontin Fault. The east block also seems to have failed in weaker material, possibly related to the fault, than the west block, which is dominated by large blocks of intact limestone. The west block failed predominantly along a biplanar surface and was kinematically controlled. Its behaviour during failure was influenced by the active-passive mechanism, the bowl-shaped failure surface, and the east-plunging south limb of the Erto Syncline, which guided movement to the north-east. The west block may have acted as a buttress, preventing failure of the east block until it had moved, thus creating the kinematic freedom necessary for the second failure. Therefore, although 2D cross-sections may indicate that the east block is equally or less stable than the west block, 3D models indicate the required kinematic freedom prior to failure of the eastern slope.

The kinematic role of the Massalezza Gully remains unclear. The 3DEC models suggest that the west block fails more easily when the failure mass is separated by the gully than the fold-related discontinuity in the east-central area. However, field and aerial photograph interpretations clearly show that the Massalezza Gully remained intact during sliding and that the smaller east block overrode the larger west block. The Massalezza could, however, have been important in the initial stages of slope instability. As the failure developed, weaker shear zones in the east could have surpassed the Massalezza zone in importance. Future investigations will include sensitivity analyses of friction and water pressures on these release surfaces.

Block size is one of the most significant parameters in all models, as demonstrated previously by Corkum & Martin (2004). Both the UDEC and 3DEC

results indicate that failure geometry, mechanism, and stability change as block size changes. Increasing the number of blocks in the 3DEC models was required for failure to occur. As block size decreased, the mechanism in two and three dimensions changed from active-passive to semi-independent displacement of individual blocks. Realistic simulation requires several blocks to be included; however, more investigation using field observations is required to determine the actual number of blocks involved.

Attempts to model the Vajont Slide include significant challenges with respect to both model and parameter uncertainties, especially in the case of three-dimensional modelling. The challenges include deciding how much detail to incorporate in the models, and model geometry and material properties. The exploratory modelling that we performed aided in identifying important characteristics. For example, incorporating the complex topography in the Slope Model simulations did not increase accuracy, and topography may have been well-represented by the simplified forms used in the 3DEC models. Including the stratigraphy in the Phase2 models did not appear to significantly influence results when the failure surface was incorporated, and the stratigraphy was reasonably approximated by using the weakest unit throughout the slide mass. Of course, the level of detail included in any model depends on the research question to be answered. For our purposes, high levels of detail were considered inappropriate given the level of uncertainty and the objectives of the study. The two main sources of uncertainty in the models are parameter and model uncertainty. Parameter uncertainty relates to the input properties used in the modelling. Despite the large amount of research on Vajont, material and discontinuity properties remain poorly constrained. We performed sensitivity analyses on important properties such as friction angle and elastic modulus, and different geometries were investigated to examine the effects of properties on stability. Our models are forensic back-analyses, with the objective of validating and constraining simulations. We did not analyse model uncertainty in this study. We implemented different constitutive models in each code, and used continuum and discontinuum codes, but a comparison of the codes was not the principal objective of the paper.

Preliminary exploratory modelling in Phase2, UDEC, 3DEC, and Slope Model highlights a number of characteristics of the Vajont Slide. The low friction angles required for failure along the sliding surface indicate that pore water pressures, kinematic freedom, and clay layers were important in enabling failure. Kinematics and block size are also important factors, both in two and three dimensions. The smaller the blocks within the sliding mass, the less stable the slope becomes. The mechanism also changes from an active-passive mode to sliding of individual blocks as block size decreases. To occur as an active-passive, catastrophic failure, the Vajont slide mass must have comprised large blocks separated by shear or joint surfaces as suggested by Hendron & Patton (1985), yet these large blocks enabled movement. Finally, the internal deformation of the slide mass, in the form of shear strain concentrations within the Prandtl wedge zone (Phase2 and UDEC) and tensile failure clusters (Slope Model) contributed to the disintegration of the failed mass into smaller blocks and decreased stability. Future work includes explicitly including groundwater, using deformable blocks, investigating the variation of shear zone thickness, and incorporating more sophisticated fracture network geometries.

ACKNOWLEDGEMENTS

Research was funded by an NSERC scholarship to A. Wolter and NSERC Discovery Grants to D. Stead and J.J. Clague. The authors thank A. Bistacchi for providing the GoCAD model for numerical modelling, and Loren Lorig and John Read for providing the Slope Model code. Slope Model was developed as part of the Large Open Pit (LOP) project, which is sponsored by Anglo-American, AngloGold Ashanti, Barrick, BHP Billiton, Compañia Minera Doña Ines de Collahuasi, De Beers, Newcrest, Newmont, Ok Tedi Mining Ltd., RioTinto, Teck Resources Ltd, Vale, and Xstrata Copper.

REFERENCES

Bandis S., Lumsden A.C. & Barton R.D. (1983) - *Fundamentals of rock joint deformation.* International Journal of Rock Mechanics and Mining Sciences & Geomechanics Abstracts, **20** (6): 249-268.

Bosa S. & Petti M. (2011) - *Shallow water numerical model of the wave generated by the Vajont landslide.* Environmental Modelling & Software, **26** (4): 406-418.

 © 2013 Sapienza Università Editrice

Broili L. (1967) - *New knowledges on the geomorphology of the Vaiont Slide slip surfaces.* Felsmechanik und Ingenieurgeologie, **5** (1): 38-88.

Corkum A.G. & Martin C.D. (2004) . *Analysis of a rock slide stabilized with a toe berm: a case study in British Columbia, Canada.* International Journal of Rock Mechanics & Mining Sciences, **41**: 1109-1121.

Ferri F., Di Toro G., Hirose T., Han R., Noda H., Shimamoto T., Quaresimin M. & De Rossi N. (2011) - *Low- to high-velocity frictional properties of the clay-rich gouges from the slipping zone of the 1963 Vaiont slide, northern Italy.* Journal of Geophysical Research, **116**: B09208, doi:10.1029/2011JB008927.

Ghirotti M. (1992) - *Aspetti geomeccanici e modellazione numerica della frana del Vajont.* PhD thesis, Universitá di Parma, Ferrara, Firenze e Pavia, Italy.

Ghirotti M. (1994) - *Nuovi dati sulla frana del Vaiont e modellazione numerica.* Geologica Romana, **XXX**: 207-215.

Goodman R.E. & Shi G. (1985) – *Block theory and its application to rock engineering*. Prentice Hall, Englewood Cliffs, NJ, USA, 338 pp.

Havaej M., Stead D., Lorig L. & Vivas J. (2012) – *Modelling rock bridge failure and brittle fracturing in large open pit rock slopes.* Proceedings of the 46th US Rock Mechanics/Geomechanics Symposium, 24-27 June 2012, Chicago, IL.

Hendron A.J. & Patton F.D. (1985) - *The Vaiont Slide: a geotechnical analysis based on new geologic observations of the failure surface.* US Army Corps of Engineers, Technical Report GL-85-5, 324 pp.

Hocking G. (1976) - *A method for distinguishing between single and double plane sliding of tetrahedral wedges.* International Journal of Rock Mechanics and Mining Science Geomechanical Abstracts, **13**: 225-226.

Itasca (2012a) - 3-*Dimensional Distinct Element Code (3DEC, v. 4.1).* Itasca Consulting Group, Minneapolis, MN, USA.

Itasca (2012b) - *Slope Model. Itasca Consulting Group,* Minneapolis, MN, USA.

Itasca (2012c) - *Universal Distinct Element Code (UDEC, v.5.0).* Itasca Consulting Group, Minneapolis, MN, USA.

Lorig L., Cundall P.A., Damjanac B. & Emam S. (2010) − *A three-dimensional model for rock slopes based on micromechanics.* Proceedings of the 44th US Rock Mechanics Symposium and 5th US-Canada Rock Mechanics Symposium, 27-30 June 2010, Salt Lake City, Utah.

Martin C.D. & Kaiser P.K. (1984) - *Analysis of a rock slope with internal dilation.* Canadian Geotechnical Journal, **21**(4): 605-620.

Martinis B. (1978) - *Contributo alla stratigrafia dei dintorni di Erto-Casso (Pordenone) ed alla conoscenza delle caratteristiche strutturali e meccaniche della frana del Vajont.* Memorie di Scienze Geologiche, Universitá di Padova, **32**: 1-33.

Mencl V. (1966) - *Mechanics of landslides with non-circular slip surfaces with special reference to the Vaiont slide.* Geotechnique, **16** (4): 329-337.

Müller L. (1968) - *New considerations on the Vaiont Slide.* Felsmechanik und Ingenieurgeologie, **6**: 1-91.

Paronuzzi P. & Bolla A. (2012) - *The prehistoric Vajont rockslide: an updated geological model*. Geomorphology, **169-170**: 165-191.

Rocscience (2012) - *DIPS (V. 6.0) & Phase2 (v. 8.0).* Rocscience Inc., Toronto, ON, Canada.

Semenza E. (2010) - *The story of Vaiont told by the geologist who discovered the landslide.* K-flash ed., Ferrara. 205 pp. [available at www.k-flash.it].

Sitar N. & Maclaughlin M.M. (1997) – *Kinematics and discontinuous deformation analysis of landslide movement.* Proceedings of the 2nd Panamerican Symposium on Landslides, Rio de Janeiro, Brazil, 65-73.

Superchi L. (2012) – *The Vajont Rockslide: new techniques and traditional methods to re-evaluate the catastrophic event.* Ph.D thesis, Università degli Studi di Padova, Italy, 187 pp.

Tika T.E. & Hutchinson J.N. (1999) - *Ring shear tests on soil from the Vaiont slide slip surface.* Geotechnique, **49** (1): 59-74.

Ward S.N. & Day S. (2011) - *The 1963 Landslide and Flood at Vaiont Reservoir Italy: A tsunami ball simulation.* Bollettino della Società Geologica Italiana, **130**: 16-26.

Wolter A., Stead D. & Clague J.J. (submitted) - *A morphologic characterisation of the 1963 Vajont Slide, Italy, using long-range terrestrial photogrammetry.* Geomorphology.